A Multiband FSS Director Using Aperture Interdigital Structure for Wireless Communication Systems

P. CHOMTONG [1], (Member, IEEE), **P. KRACHODNOK** [2], (Member, IEEE), **K. BANDUDEJ** [3], **AND P. AKKARAEKTHALIN** [4], (Member, IEEE)

[1] Department of Teacher Training in Electrical Engineering, Faculty of Technical Education, King Mongkut's University of Technology North Bangkok, Bangkok 10800, Thailand

[2] School of Telecommunication Engineering, Institute of Engineering, Suranaree University of Technology, Nakhon Ratchasima 30000, Thailand

[3] National Astronomical Research Institute of Thailand (NARIT), Chiang Mai 50180, Thailand

[4] Department of Electrical and Computer Engineering, Faculty of Engineering, King Mongkut's University of Technology North Bangkok, Bangkok 10800, Thailand

Corresponding author: P. Krachodnok (priam@sut.ac.th)

ABSTRACT This research paper proposes a multi-band frequency selective surface (FSS) director using the aperture interdigital technique. The FSS unit cell has been designed based on a basic bandpass filter (BPF) connected with an interdigital structure. With the proposed structure, the FSS unit cell size can be reduced from $\lambda/2$ to $\lambda/8$ caused by the slow-wave effect of interdigital capacitance loaded at the end of the transmission line in the unit cell structure. Moreover, the capacitance loaded at the end of the transmission line can control the second and the third resonance frequencies to resonate as required. The unit cell has been designed at the fundamental frequency of 1.8 GHz and the controlled second and third resonance frequencies of 3.7 GHz and 5.2 GHz, respectively. The operating frequencies of the proposed FSS unit cell cover LTE band (0-1.9 GHz), Wi-MAX band (3.22GHz-4.7GHz), and WLAN band (5.15 GHz-5.95 GHz). The size of the unit cell is very compact which is 11.53 mm $\times$ 10.77 mm. The designed unit cells are then connected as an array of 8 $\times$ 8, resulting in an overall size of 92.31 mm $\times$ 86.16 mm. This array has been used as a director for dipole antennas designed at the frequencies of 1.8 GHz, 2.45 GHz, 3.7 GHz, and 5.2 GHz. From the simulation, the dipole antennas with the proposed FSS director have directional gains of 4.52 dB at 1.8 GHz, 3.83 dB at 3.7 GHz, and 3.29 dB at 5.2 GHz, respectively. Measurement results show the directional gains of 3.67 dB at 1.8 GHz, 3.16 at 3.7 GHz, and 3.42 dB at 5.2 GHz, respectively. The proposed FSS director has properties of multi-band operation with a compact size that can be developed for antenna covers and radomes of multi-band wireless communications.

INDEX TERMS Multiband, frequency selective surface, FSS antenna director, aperture interdigital structure.

I. INTRODUCTION

Nowadays, advanced wireless communications are constantly developing to support such a wide variety of usage volumes, especially 5G mobile communications and wireless local area network systems or even satellite communications. Wireless communications must require high speed and good quality transmission. Antennas are one of the essential parts

The associate editor coordinating the review of this manuscript and approving it for publication was Kuang Zhang.

of all wireless communication systems to be designed to transmit and receive electromagnetic waves. So, the major developments of antennas are often to increase radiation efficiency and gain, resulting in increasing the communication capacity and distance. In addition, the size of the antenna has been reducing to be significantly smaller, allowing it to be used effectively with various systems. To date, metamaterials had been developing to be used to enhancing antenna efficiency. The metamaterial has a material property that does not exist naturally by changing the value of electrical

permeability to be negative value [1], [2]. According to the desired multi-band operations, multi-band metamaterials have been studied [3], [4]. A multi-band metamaterial reflector for dipole antennas has recently been designing [5], resulting in efficiency and gain improvement. Another method for increasing the antenna efficiency is to use an electromagnetic bandgap (EBG) structure [6]–[8]. The EBG can eliminate surface waves on the material surface, resulting in only appeared wave propagation. However, the EBG can increase the efficiency and gain of the antenna when it can only be a reflector. In addition, a technique of frequency selective surface (FSS) using a metamaterial surface has been proposed. The FSS can select a frequency range of signals to transmit or reflect. The FSS is suitable to be applied for connecting with an antenna to increase the threshold capable of transmitting antenna propagation without distorting the diffusion at a frequency range due to the coupling material. Therefore, the FSS is popularly used because it is easy to design as either a reflector or a director. It can be designed to respond to a wide range of frequencies depending on the structures. The FSSs have been studied for a wide variety of applications. The FSS associated with square patch unit cells was designed to be an antenna reflector with a structure size of approximately $\lambda/2$ and responding to only a single frequency [9]. Afterward, the FSS reflector was designed to increase the bandwidth for reflecting the antenna, enabling the antenna to use at the specified frequency, however, the size was still large [10], [11]. The FSS reflector was then designed to be compatible with wideband antennas used to enable multi-band operation but the structure was also large and very complex. Later, there was the proposed FSS reflector design with slot ground antenna using a double layer structure of ring resonators [12], [13]. The FSS has a wideband resonance which the unit cell structure of the reflector is approximately $\lambda/2$. This causes the reflector to be large and the gain of the antenna is still low. The FSSs for transmission have been also studied in a variety of formats such as characterization of a single unit cell or the FSS layer to enable multi-band frequency responses [14]–[17] and changing the impedance of structure to achieve multi-band frequency [18]–[20] but the design has a complex structure and the size of the unit cell is also large. From the above researches, it can be seen that the design of the FSS is as important as the design of the structure which the structure can be designed with microwave circuit design technique. It is possible to design smaller unit cells and control resonance frequencies for use in a multi-band operation [21]–[23]. This paper proposes a design of the multi-band FSS director which is based on a bandpass filter (BPF) with interdigital structure, [24]–[27] since it has the advantage of being able to control the second resonance frequency to the desired frequency [28]–[33]. This unit cell is designed at the fundamental frequency of 1.8 GHz, the second resonance frequency of 3.7 GHz, and the third resonance frequency of 5.2 (LTE, Wi-MAX, and WLAN). The unit cells will be connected to act as the FSS array applied for a single band dipole antenna radiated at 1.8 GHz, 2.45 GHz, 3.7 GHz,
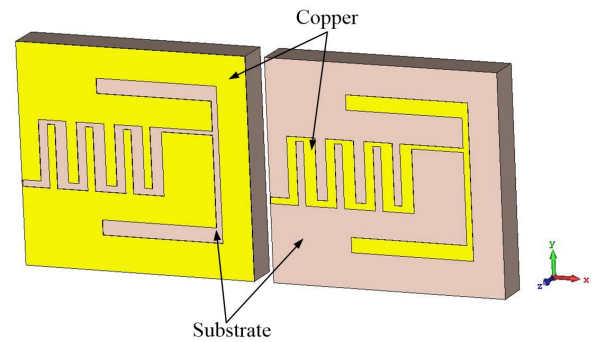

FIGURE 1. The normal unit cell (left) compared with the proposed structure (right).
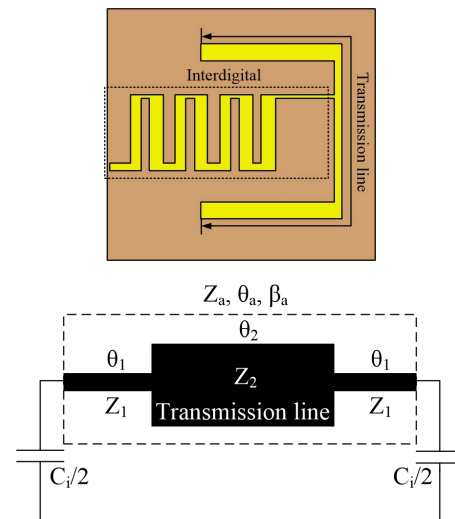

FIGURE 2. The proposed unit cell and parameters of the equivalent circuit.

and 5.2 GHz (one antenna one frequency). The distance between the antenna and the FSS array is approximately $\lambda/8$. The FSS array is radiated through all frequencies from the resonant antenna. This paper is divided into three sections, the first part proposes the unit cell design, the second part proposes the simulation results of the FSS unit cell connect to an array with a dipole antenna and the third part is the measurement results in the design of FSS director.

II. DESIGN OF THE UNIT CELL

This part proposes the design of the FSS unit cell, based on a multiband BPF structure connected with an interdigital section without a ground plane [31], [32]. Then, the unit cells can be arranged to form an array as FSS. When used with a radiator, the signals can transmit through the FSS with some gains. The proposed structure of the FSS unit cell is shown in Fig. 1. It can be clearly seen that the proposed unit cell is the inverted structure of the normal unit cell, in which copper and aperture are switched. It is also found that both unit cells have the same characteristics.

The unit cell uses the step-impedance technique [26], [27] for controlling the second resonance frequency together with
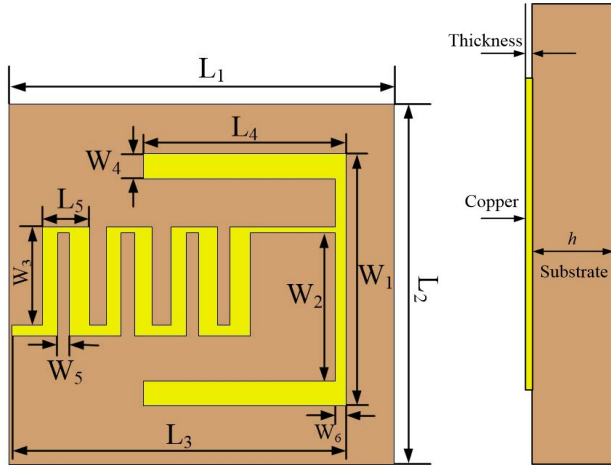
FIGURE 3. The parameters of the unit cell.

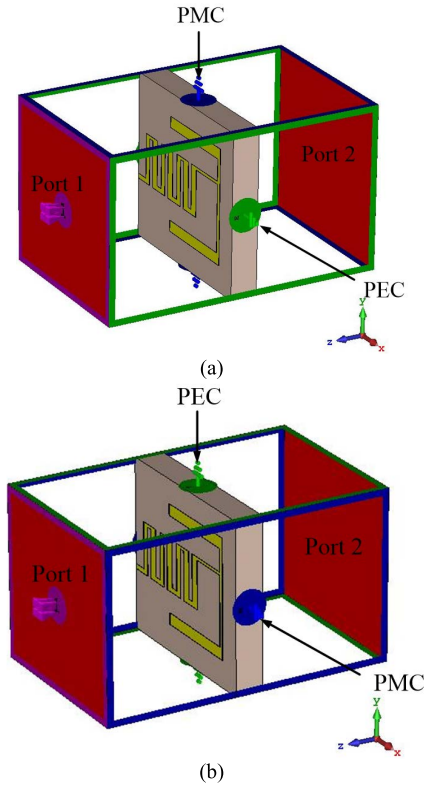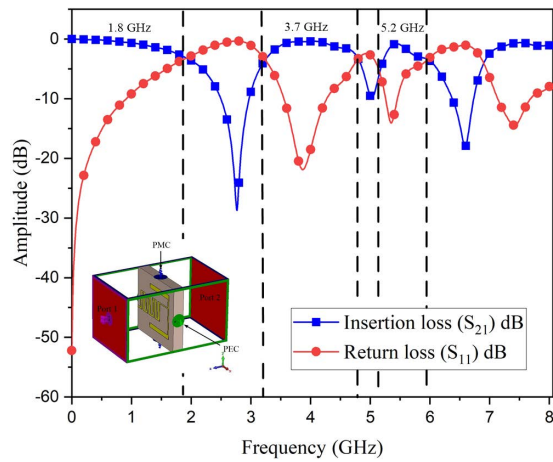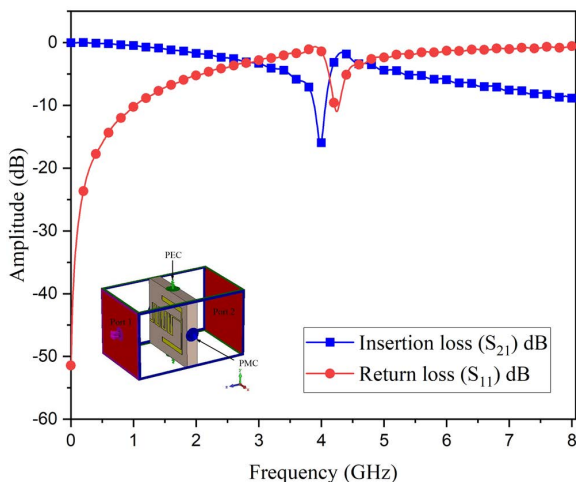| Parameters	
W_1 = 7.53 mm.	L_1 = 11.53 mm.
W_2 = 4.43 mm.	L_2 = 10.77 mm.
W_3 = 2.96 mm.	L_3 = 10.18 mm.
W_4 = 0.73 mm.	L_4 = 6.05 mm.
W_5 = 0.38 mm.	L_5 = 1.40 mm.
W_6 = 0.66 mm.	h = 1.6 mm.

FIGURE 4. The simulation configurations of the unit cell with (a) E- field on the x polarization wave (b) E- field on the y polarization wave.

the interdigital technique at the end of the transmission line. Fig. 2 shows the proposed structure of the unit cell consisting of a transmission line connected to the interdigital part and also its equivalent circuit with key parameters. In this work, the unit cells are designed at the fundamental frequency (f_0) of 1.8 GHz, while the controlled second (f_1) and third (f_2) resonance frequencies are at 3.7 GHz and 5.5 GHz, respectively applicable for LTE, Wi-MAX, and WLAN systems. From the equivalent circuit, when increasing the loaded capacitive value of the interdigital part (C_i) at the end of the transmission line, it can control the second and third resonance frequencies shifted to desired frequencies [24]. This can be effectively achieved by using the step-impedance technique, in which all important parameters can be calculated as in (1) - (1) [28].

$$\theta_{a0} = 2\tan^{-1}\left(\frac{1}{\pi f_0 Z_a C_i}\right)$$

$$\theta_{a1} = 2\pi - 2\tan^{-1}\left(\pi f_1 Z_a C_i\right)$$

$$\theta_{a2} = 2\tan^{-1}\left(\frac{1}{\pi f_2 Z_a C_i}\right)$$

$$Ci = \frac{(\varepsilon_r + 1)}{L_4} W_3 (\varepsilon_r + 1)\left[0.1(n-3) + 0.11\right]$$

$$\frac{1}{Z_a} = jY_a \frac{2(1+K)\left(K - \tan^2\theta_a\right)\tan\theta_a}{K - 2\left(1 + K + K^2\right)\tan^2\theta_a + K\tan^4\theta_a} \quad (1)$$

when

$$K = \frac{Z_2}{Z_1}.$$

As seen in (1), θ is the electrical length for the resonant frequency when the given values of θ_{a0}, θ_{a1}, and θ_{a2} are electrical lengths on the transmission line at the fundamental frequency, the second and the third resonance frequencies, respectively. They can be described as the loaded capacitive of the interdigital part (C_i) at the end of the transmission line. This only has a little effect on harmonic frequency, but it has an important effect on the fundamental frequency. It is found that increasing the capacitive value causes the shifted resonant frequencies, shifting the frequency f_1 more

than the frequency f_2. In addition, the value of Z_a, which is the impedance of the transmission line, also has more effect on the second resonance frequency. The transmission line using the step-impedance technique consists of parameters, in which θ_a is the total electrical length on the transmission line and β is the propagation constant of the transmission line. In case the second and third frequency resonance control is required, the step-impedance structure consists of two sections of the transmission lines including impedance parameters Z_1 and Z_2. θ_0 and θ_1 are the electrical lengths corresponding to Z_1 and Z_2, respectively. When the impedance in the transmission line Z_1 larger than Z_2, the K ratio will affect f_1 shifted away from f_0 [27]–[32]. Fig. 3 shows some
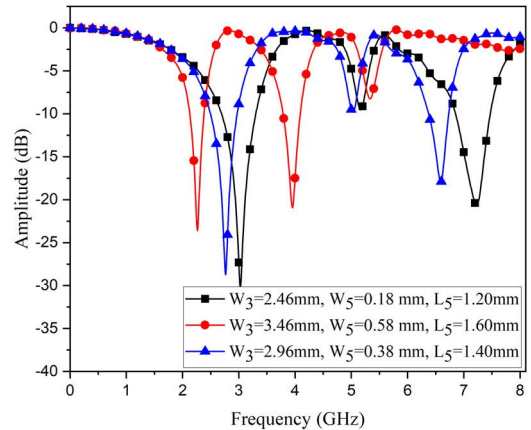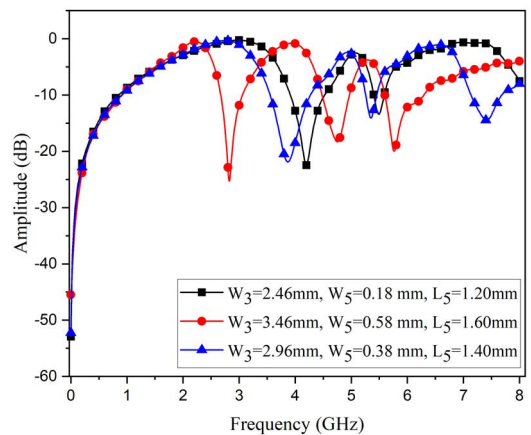
FIGURE 5. The simulation results of the unit cell when setting the configurations (a) E- field on the x polarization wave (b) E- field on the y polarization wave.

FIGURE 6. The simulation results of the unit cell using interdigital structure (a) insertion losses (S21) and (b) return losses (S11).

important parameters of the proposed unit cell. The unit cell of the FSS was designed on an FR-4 print circuit which has ε_r of 4.4 thickness of 0.035 mm, a substrate high of 1.6 mm, loss tangent of 0.025. The first dimension of this design is given in Table 1. To increase or decrease capacitive load values depending on the size and number of interdigital fingers, the unit cell parameters of L_5, W_3, and W_5 must be carefully adjusted. In addition, when increasing the loaded capacitive value, it will shift the second and the third resonant frequencies because the electrical length on the transmission line increases and is not equal to the physical length. Therefore, to make the resonant frequency shift back to the original frequency range, the size of the transmission line has to be reduced.

Form the proposed structure, the size of the transmission line can be reduced from $\lambda/2$ to $\lambda/8$ at the fundamental frequency of 1.8 GHz. This means that using the capacitive-loaded structure can reduce the size of the unit cell. The value of C_i can be calculated by (1) when n is the number of fingers. The impedance in the transmission line can be

calculated according to (1). From the above design, the unit cell has been simulated using the CST Studio Suit program to obtain the transmission characteristics. In the program, the unit cell is arranged in the z-axis and the electric field (E-field) and magnetic field (H-field) in the x-axis and the y-axis are alternately configured corresponding to the currents as shown in Fig. 4. It was found that the resonance frequency is at f_0, while the harmonic frequencies of f_1 and f_2 can be controlled when configuring the E-field and the H-field as in Fig. 4(a). The results of frequency responses for this configuration are shown in Fig. 5(a). However, when configuring the E-field and the H-field as in Fig. 4(b), the unit cell ack as a bandpass filter on both harmonic frequencies, therefore they are unable to control for achieving desired resonance frequencies. The results of frequency responses for this configuration are shown in Fig. 5(b). This means that when applying the unit cells as FSS for the antenna system, the antenna must be placed along the x-axis so that the harmonic frequencies can be controlled.

It is found that the loaded capacitive value at the end of the transmission line must be varied by increasing or decreasing the finger and gap parameters to control the second and the third resonance frequencies of the proposed unit cell.
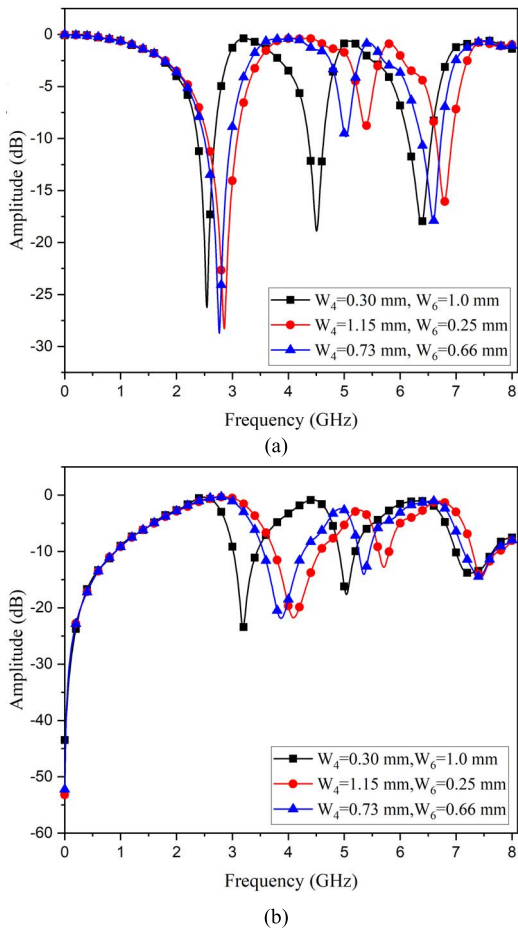
(a)

(b)

FIGURE 7. The simulation results of the unit cell using step-impedance structure (a) insertion losses (S21) and (b) return losses (S11).

FIGURE 8. The simulated E-field results of the unit cell at (a) 1.8 GHz, (b) 3.7 GHz, and (c) 5.2 GHz.

FIGURE 9. The simulated H-field results of the unit cell at (a) 1.8 GHz, (b) 3.7 GHz, and (c) 5.2 GHz.

Therefore, the interdigital part parameters including L_5, W_3, and W_5 were studied by using CST simulation by increasing and decreasing the parameters as shown in Fig. 6. It is clearly seen that decreasing the loaded capacitive value effects the harmonic resonance frequencies of f_1 and f_2 shifted away from the fundamental frequency of f_0. This can be noticed on the graphs that the harmonic resonance frequencies are shifted from left to right (blue and black lines) as the loaded capacitive decreased. However, increasing the loaded capacitive value will affect the harmonic resonance frequencies of f_1 and f_2 moved toward the fundamental resonance frequency of f_0. The results will be applied to the final design of the proposed unit cell.

In our design, the second and third resonance frequencies are moved closer to the fundamental frequency of f_0 as a result of capacitive value increment, therefore the electrical length on the transmission line is not equal to the physical length. If the fundamental resonance frequency is designed to resonate at the original frequency, the length of the transmission line must be reduced to lesser than half its original wavelength. It is found that the length of the transmission line can be reduced from $\lambda/2$ to $\lambda/8$. In addition, to design the unit cell having the second and the third resonance frequencies
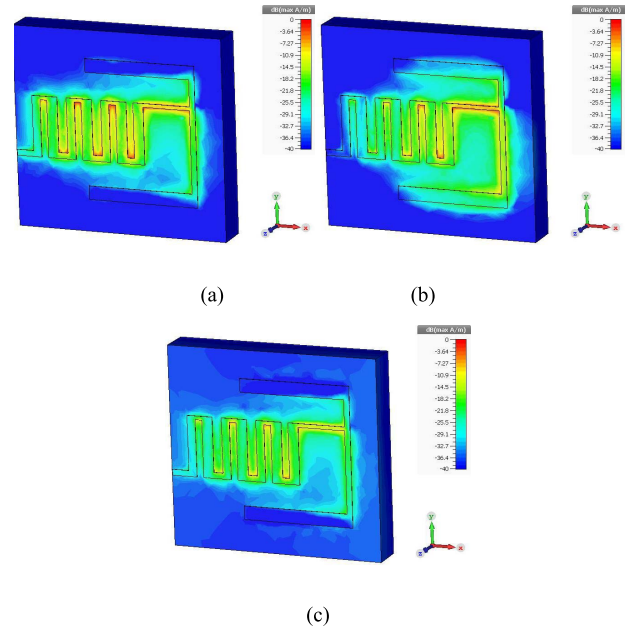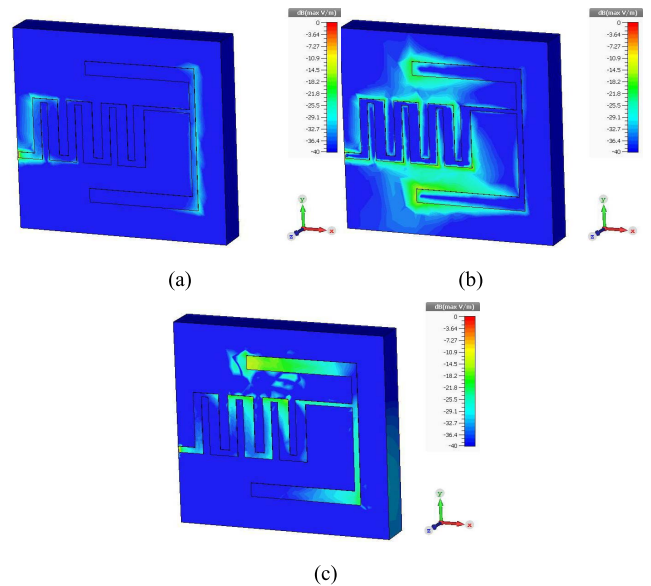
to be able to resonate at the desired frequencies, the step-impedance technique on the transmission line is used together with the interdigital structure. By using the step-impedance technique, the harmonic frequencies can be further controlled. Therefore, the key parameters of the step-impedance structure of W_4 and W_6 were studied using the CST simulation as the result shown in Fig. 7.

Form Fig. 7, it is found that when using technique step-impedance with the ratio between Z_1 and Z_2 or ratio of K > 1, it will cause frequencies of f_1 and f_2 to shift away from the frequency of f_0, which has a great effect in shifting the
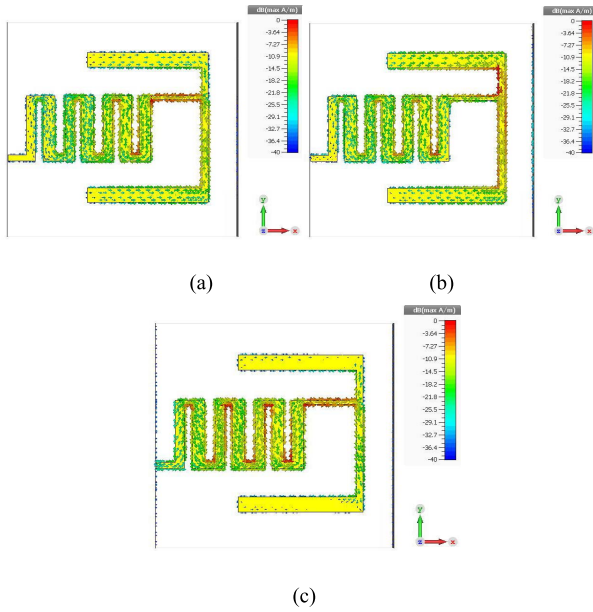
FIGURE 10. The simulated current density results of the unit cell at (a) 1.8 GHz, (b) 3.7 GHz, and (c) 5.2 GHz.
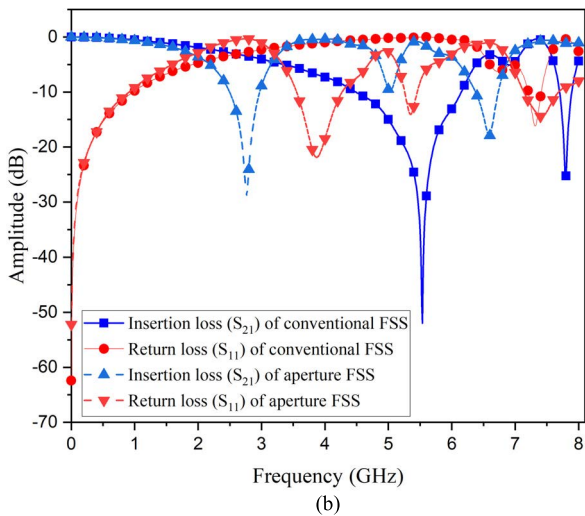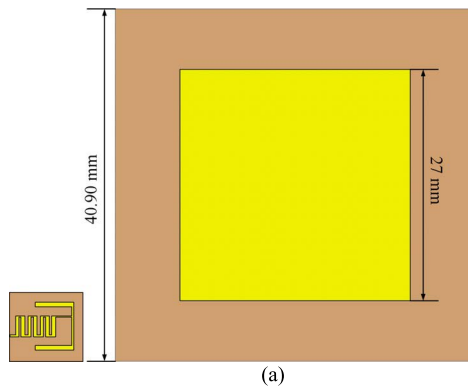

FIGURE 11. Comparison between the conventional and the proposed FSS unit cells (a) structure sizes and (b) simulated results of insertion and return losses.
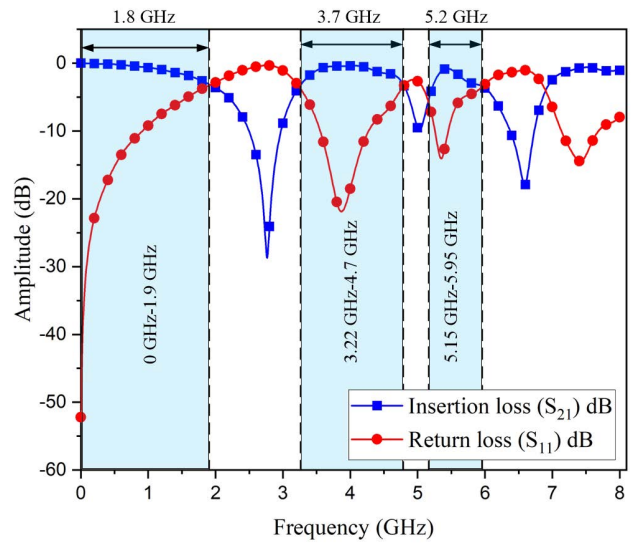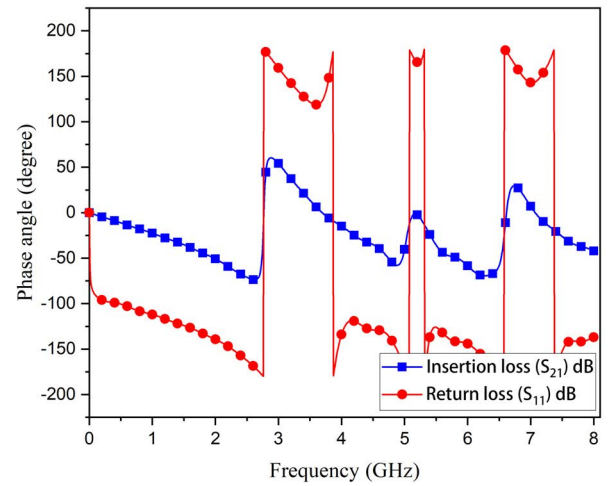

FIGURE 12. The simulated results of an FSS unit cell. (a) phase responses and (b) resonance frequencies and bandwidths.

TABLE 2. Dipole antenna dimension.

Dipole parameters	Dimension (mm)		
	f = 1.8 GHz	f = 3.7 GHz	f = 5.2 GHz
L_d	32.50	13.80	8.40
L_t	68.00	29.60	16.80
G_d	3.00	2.00	2.00
W_1	3.46	3.46	3.46
T	0.46	0.46	0.46

second resonance frequency as shown in the red line. If Z_1 and Z_2 or ratio of K < 1, it will cause the frequencies of

f_1 and f_2 to shift closer to the frequency of f_0 as shown in the black line. In our design, the suitable impedances for producing the desired resonance frequencies include $Z_1 = 100$ ohms and $Z_2 = 133$ ohms. After designing the unit cell,
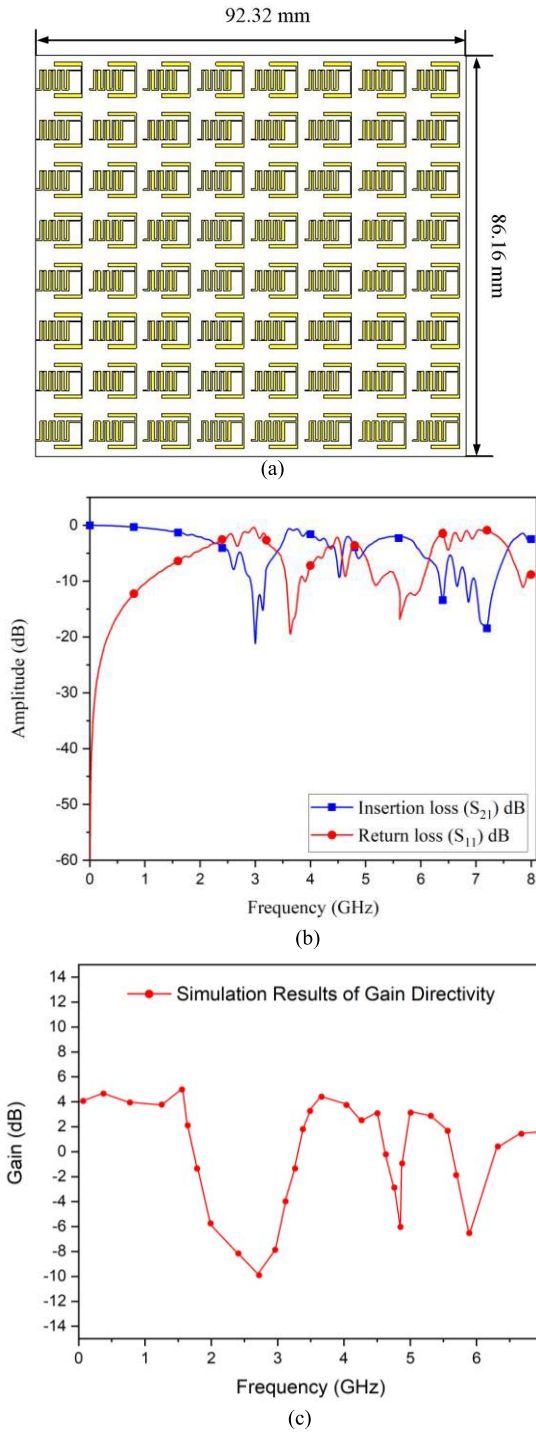
(a)

(b)

(c)

FIGURE 13. (a) the structure of FSS with 8 × 8 unit cells (b) the simulated results and (c) the simulations result of gain.

FIGURE 14. The geometry of single frequency dipole antenna.

(a)   (b)
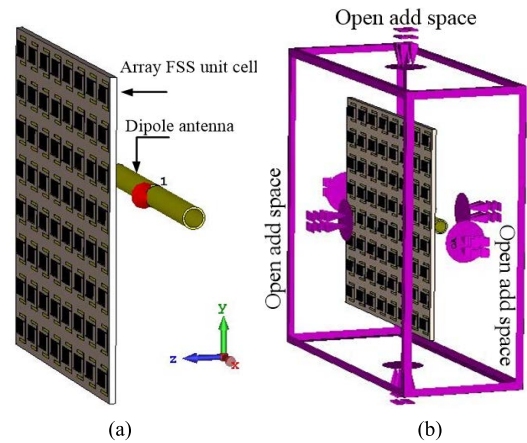
FIGURE 15. The proposed FSS (a) with the dipole antenna and (b) boundary conditions for simulation.

(a)   (b)

(c)
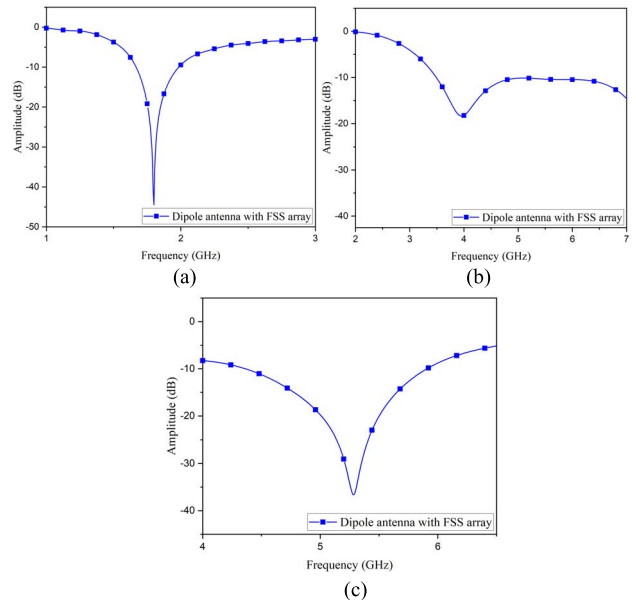
FIGURE 16. The simulated return losses of the proposed FSS with a dipole antenna at (a) 1.8 GHz, (b) 3.7 GHz, and (c) 5.2 GHz.

the E-field and H-field values on the unit cell structure were studied as shown in Fig. 8. It is found that at the resonance frequency f_0 the E-field is dense on the transmission line and the interdigital interval. At the harmonic resonance frequency of f_1, it is found that the E-field density is observed on the step-impedance transmission line and interdigital part. At the harmonic resonance frequency of f_2, it has a density
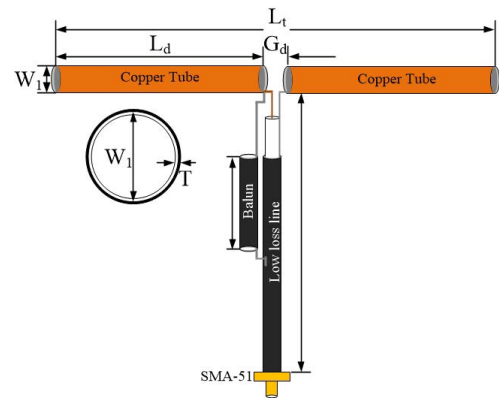
of the E-field as same as the resonant frequency of f_0. The results from the simulation are consistent with the equation and simulation results as mentioned above.
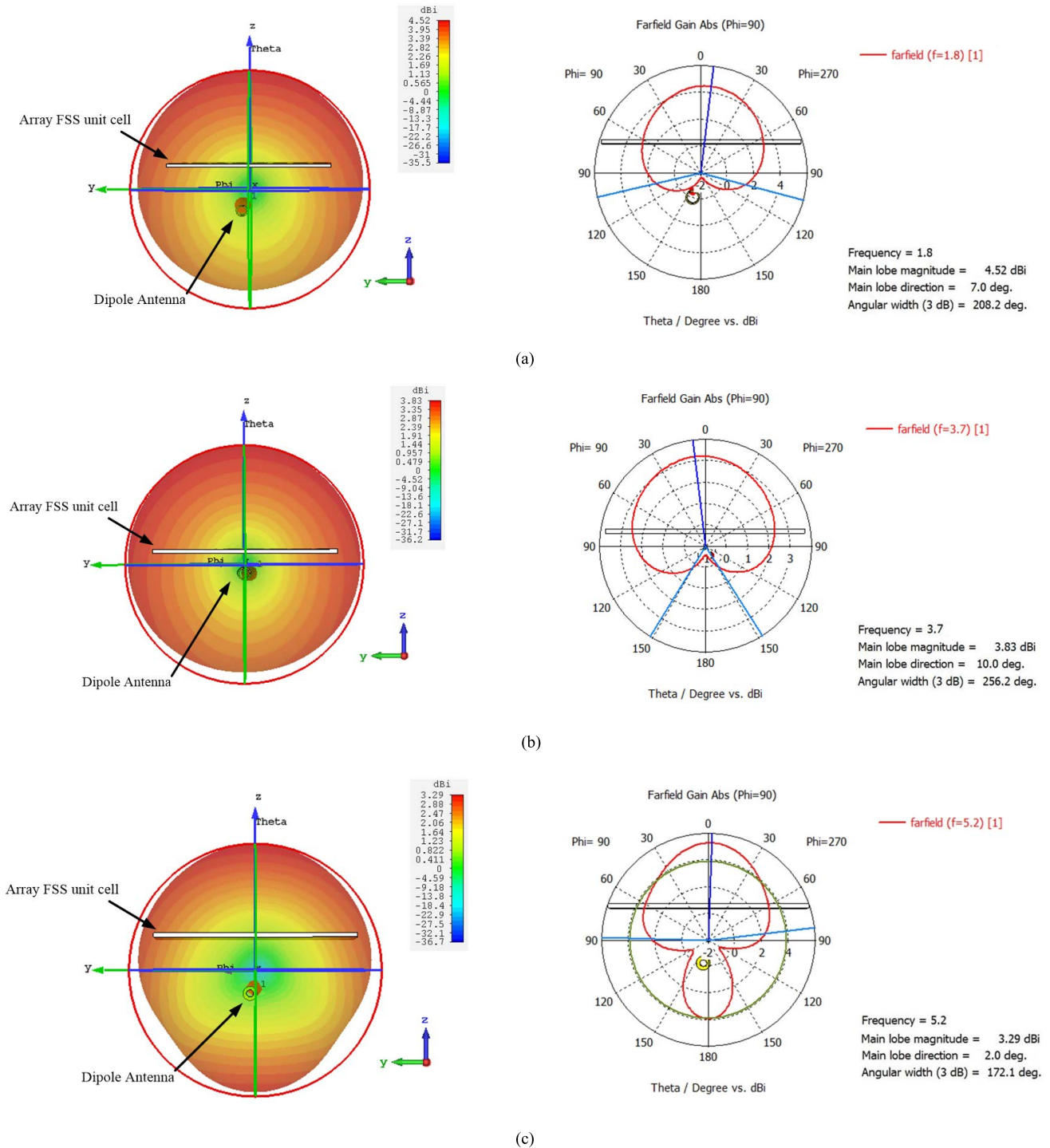
(a)

(b)

(c)

FIGURE 17. The simulated radiation patterns and gains of the dipole antenna with the FSS at (a) 1.8 GHz, (b) 3.7 GHz, and (c) 5.2 GHz.

The H-field density on the structure of the unit cell was studied by CST simulation as the results shown in Fig. 9. It is found that at all resonant frequencies, the transmission line and the interdigital intervals have fewer H-field densities compared with the E-field densities due to the arrangement of the unit cell structure.

Then the current distribution on the unit cell was simulated as the results shown in Fig. 10. It is found that at resonant frequencies of f_0 and f_2, there are high current distribution in the transmission line and interdigital part. In the resonant frequency of f_1, there is more current density on the step-impedance transmission line and interdigital part.
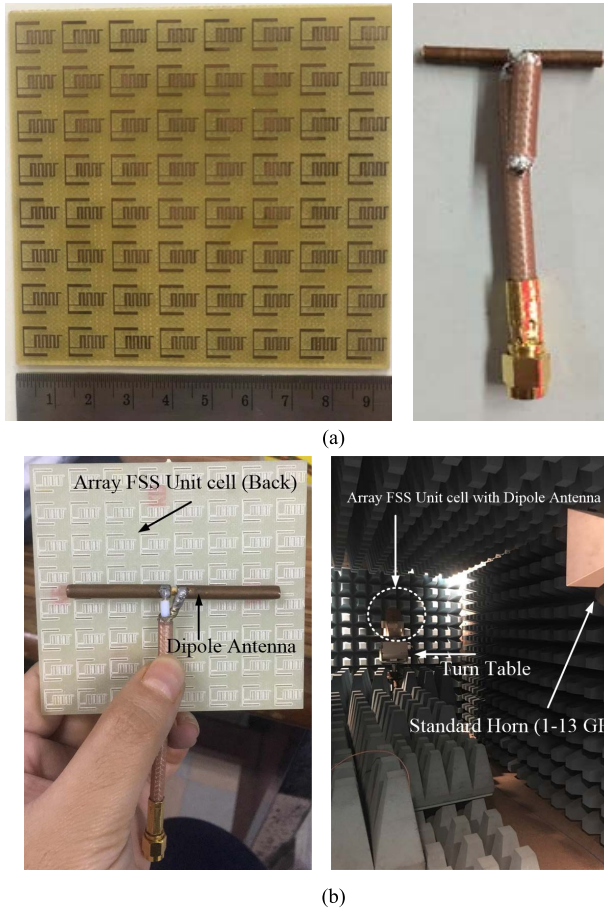
(a)

(b)

FIGURE 18. (a) The fabricated FSS and the dipole antenna and (b) the measurement setup for the antenna in chamber room.

The simulation results consistent with the design equations and directly correspond to the E-fields. When comparing the size of the proposed unit cell with the conventional metallic patch unit cell in Fig. 11, it is found that the size of the proposed unit cell is significantly smaller because of using the design techniques mentioned above. The approximate size of the proposed unit cell structure is λ/8, while the conventional structure is approximately λ/2. In addition, the proposed unit cell structure can be operated for three controlled resonance frequencies, besides the conventional metallic patch unit cell structure can only be operated for a fundamental frequency and the uncontrollable second and third resonant frequencies. Therefore, the proposed unit cell can be easily applied for a wide variety of multiband antenna applications.

In our design, the unit cell was intentionally designed to operate at the fundamental frequency of 1.8 GHz with the lowpass transmission response and the bandwidth of 1.9 GHz (0-1.9GHz). Also, it has the second resonance frequency of 3.7 GHz with the bandpass transmission response and the bandwidth of 1.48 GHz (3.22GHz-4.7GHz), and the third resonance frequency of 5.2 GHz with the bandpass transmission response and the bandwidth of 0.8 GHz (5.15GHz-5.95GHz) as shown in Fig. 12. The insertion losses at the resonance frequencies are 2.1 dB, 1.36 dB and 1.21dB, respectively, and
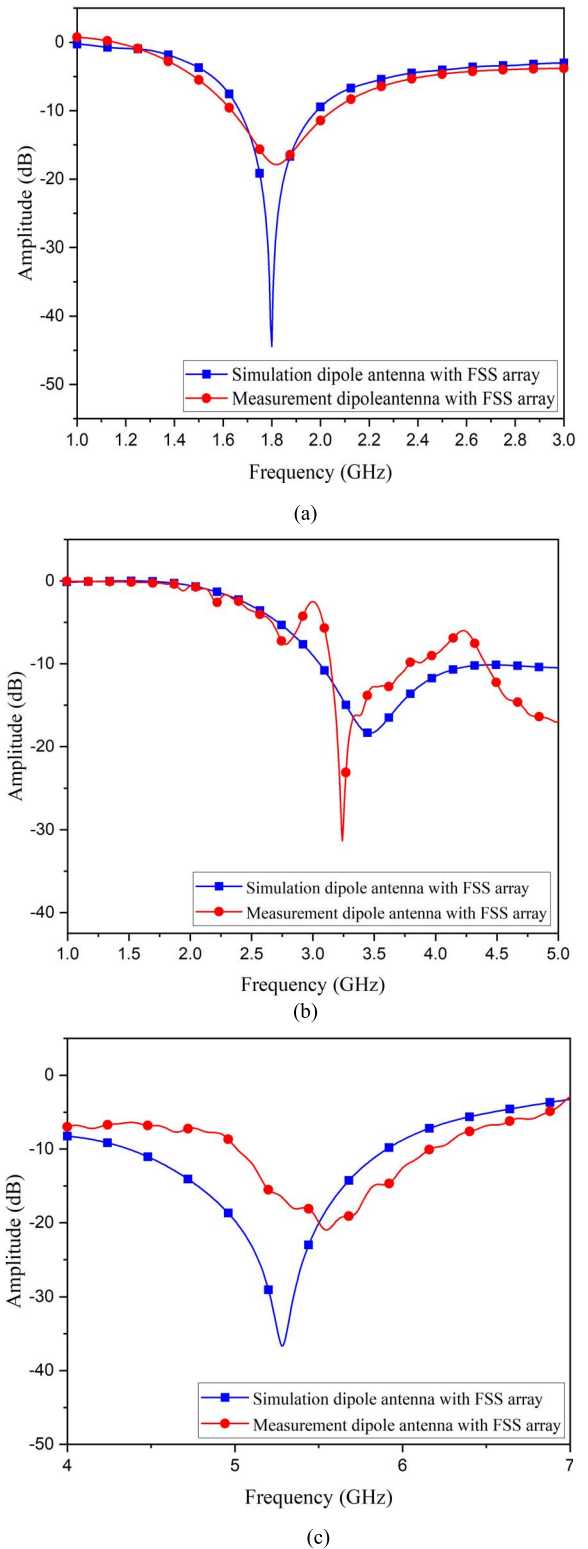

(a)

(b)

(c)

FIGURE 19. The comparison of simulated and measured insertion losses of the antenna with FSS director at (a) 1.8 GHz, (b) 3.7GHz, and (c) 5.2 GHz.

also the return losses are −7.4 dB, −23 dB and −15 dB, respectively. When comparing phase angle responses, they consistent with phase reversals for the non-transmitted phase
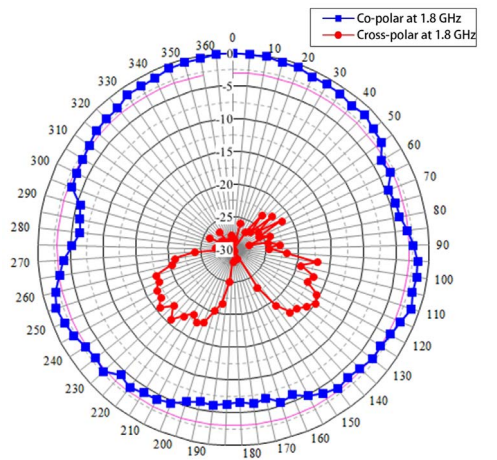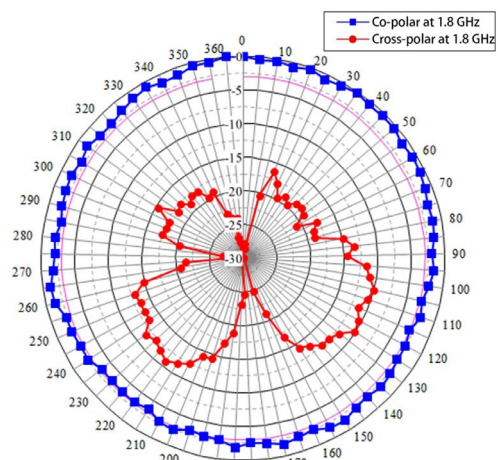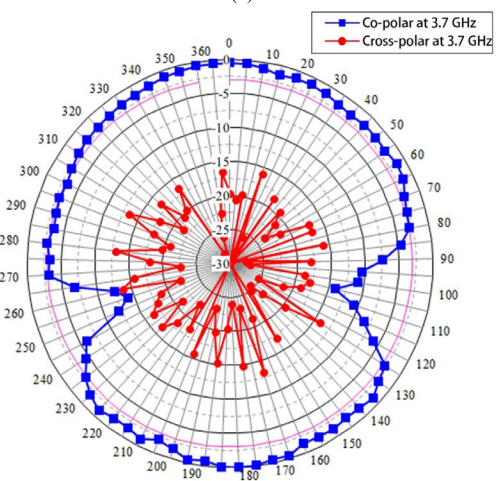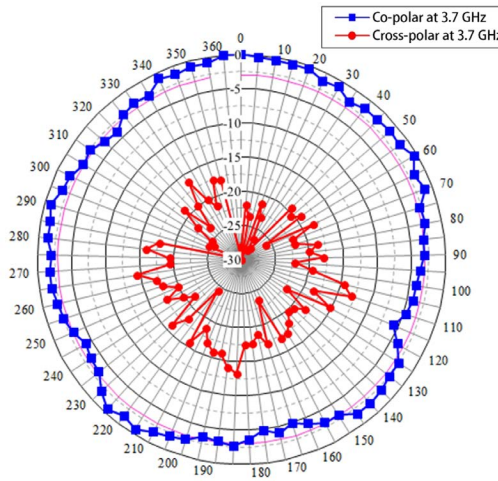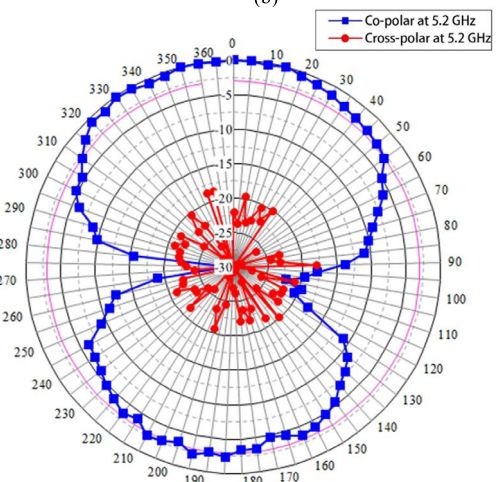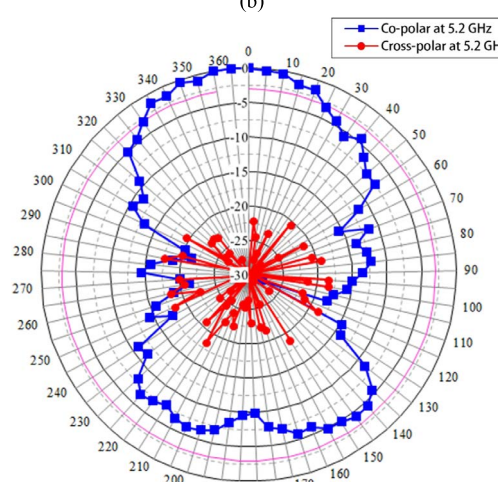
FIGURE 20. Measured results of E-plane radiation patterns at (a) 1.8 GHz, (b) 3.7 GHz, and (c) 5.2 GHz.

FIGURE 21. Measured results of H-plane radiation patterns at (a) 1.8 GHz, (b) 3.7 GHz, and (c) 5.2 GHz.

corresponding to the return losses at all resonance frequencies. This will allow all three frequencies to transmit through

the controlled frequency bands, resulting in resonance covering the LTE, Wi-MAX, and WLAN systems.

TABLE 3. Comparison of the proposed design multiband FSS with reference.

| Reference Number	No. of bands (structure shaped)	Freq.(GHz)	Unit cell size (mm³)	Overall size (mm³)	No. of unit cell array	Measurement gain (dB)	Type of Applications
[9]	1 (Square patch)	4-6 and 7-9	6 ×6×0.1	100×100	6×14	9.5	FSS Reflector
[10]	1 (2 layer cDRAs.)	5.2, 5.5 and 5.8	15.75×15.75×2.2	126×126×2.2	6×8	More 12	FSS Reflector
[11]	1 (Square slot patch)	9.6,13.4 and 17.5	10.5×5×3.524	84×5×3.524	8×1	-	Dual Polarize FSS
[12]	1 (Square patch)	3.2-12	19.5×2.8×1.6	30×60	13×5	3-4	FSS Reflector
[13]	2 (Circular loop)	2.4 5.8	25.6×1.7×1.6	25.6×1.7×1.6	1	-	FSS Control frequency
[14]	3 (Combine between Square slot and Cross patch)	4.66 9.6 20	23.25×27.5×1.6	30×30×1.6	1	-	FSS Transmission
[15]	1.0-18 (Open Matryoshka Element)	1.0-18	24×24×0.97	240×240×0.97	10×10	-	FSS Transmission
[16]	3 (Multi layer PIN Diode FSS)	1.2 2.6 4.1	20×20×1	20×20×1	1	-	FSS Transmission
[17]	1 (MUC FSS)	28-31	3.4×5.6×0.508	13×9×0.508	3×5	11 11 10.4	FSS Reflector
[18]	3 (Square patch with Square slot)	3 6 9	5.2×5.2×1 (3GHz) 1.02×1.02×1 (6GHz) 5.6×5.6×1 (9GHz)	60×60×1	7×7	7.5 9.2 7.1	FSS Reflector
[21]	1 (Chirality-assisted geometric-phase)	9-11	8.88×8.88×1	220×220×4.47	25×25	-	Meta SurfaceTransmission
[22]	1 (Ultra-thin meta-deflectors)	10	5.5×6.9×2	250×250×2	25×25	-	Meta Deflector
[23]	1 (OAM)	9.5-10.5	5.7×5.6×1	24	24 Meta atom	-	Meta Surface Angular Multiplexing
FSS proposed	3 (Interdigital)	1.8 2.45 5.2	10.77×11.53×1.6	86.16×92.32×1.6	8×8	3.67 3.16 3.42	FSS Director

III. DESIGN OF FSS DIRECTOR WITH THE DIPOLE ANTENNA

After designing the unit cell in the previous section, the proposed unit cells are connected to form an array as frequency selective surface (FSS). The number of unit cells in this array is 8 × 8 unit cells corresponding to the size of the dipole antenna as shown in Fig. 13(a). The overall size of the designed FSS array is 92.32 mm × 86.16 mm. Fig. 13(b)

shows the simulation results of the FSS array structure and Fig. 13(c) shows the simulation gain of FSS array at 1-7 GHz. It is found that the FSS can transmit the signals over the designed frequency ranges as same as the single unit cell. However, the insertion loss and return loss responses may have little differences caused by the effects from the unit cell connection. Next, a dipole antenna is designed as shown in Fig. 14 and it will be placed over the FSS array. The dipole antenna dimensions for three operating frequencies are listed in Table 2.

The dipole antennas were designed with copper metal tubes at each operating frequency of 1.8 GHz, 3.7 GHz, and 5.2 GHz. A low-loss cable and a balun were connected to the dipole antenna. From the simulation results, each dipole antenna has a return loss (S_{11}) lesser than −10 dB at the resonance frequencies and gains of the antenna are about 2 dB, 1.97 dB, and 1.86 dB, respectively. Then, the proposed FSS was employed to be a director for each dipole antenna by placing it behind the dipole as shown in Fig. 15(a). The boundary conditions around the dipole antenna and the FSS array are set as shown in Fig. 15(b). The distance between the dipole antenna and the FSS array at all resonance frequencies is about λ/8, which is very small comparing with the conventional antenna structure. The simulation results of the dipole antenna with an FSS array at all resonance frequencies are shown in Fig. 16. The is found that the return losses (S_{11}) lesser than −10 dB at 1.8 GHz with a bandwidth of 280 MHz (1.65 GHz-1.93 GHz), 3.7 GHz with a bandwidth of 780 MHz (3.52 GHz-4.30 GHz), and 5.2 GHz with a bandwidth of 740 MHz (4.63 GHz-5.37 GHz). Also, all dipole antennas can radiate through the FSS director at the resonance frequencies with increasing gains of 4.52 dB at 1.8 GHz, 3.83 dB at 3.7 GHz, and 3.29 dB at 5.2 GHz as simulation results shown in Fig. 17.

IV. MEASUREMENT RESULTS

This section proposes the implementation and testing of the dipole antenna with the proposed FSS director. The FSS director was built on the FR-4 printed circuit board and by using a milling machine process. Dipole antennas were made of copper tubes connected by a low-loss signal cable and an SMA-51 type connector, and a balun to make it a balanced line. Three dipole antennas were constructed for all three resonant frequencies. Fig. 18(a) shows pictures of the fabricated FSS director and the dipole antenna. The antenna system including the dipole antenna and the FSS director were tested in the chamber room as shown in Figure 18. Measured results show that at the three resonant frequencies, the antennas have return losses (S_{11}) lesser than −10 dB as shown in Fig. 19 similar to the simulation results. It is also found that the bandwidths are 350 MHz (1.60 GHz-1.95 GHz) at 1.8 GHz, 610 MHz (3.15 GHz-3.76 GHz) at 3.7 GHz, and 970 MHz (5.15 GHz-6.12 GHz) at 5.2 GHz. The antenna radiation patterns are also obtained at all frequency ranges as shown in Fig. 20. It is found that the co-polar plot at the resonance frequency of 1.8 GHz has omnidirectional pattern with the

maximum transmission direction at an angle of 0 degrees and the gain of 3.67 dB. At the resonance frequency of 3.7 GHz, it has a bi-directional pattern with the maximum transmission direction at an angle of 0 and 180 degrees. The antenna gain at this frequency is about 3.16 dB. Also, at the resonance frequency of 5.2 GHz, it has a bi-directional pattern with the maximum transmission direction at an angle of 0 and 180 degrees. The antenna gain at this frequency is 3.42 dB. Seen cross-polar plots, all antennas at all frequencies have poor radiation. The antenna measurement in the H-plane co polarization is shown in Fig. 21. At the resonance frequency of 1.8 GHz and 3.7 GHz, the antennas have omnidirectional patterns and the gains are increased to be 3.53 dB and 3.18 dB, respectively. Besides, at the resonance frequency of 5.2 GHz, it has a bi-directional pattern with a gain of 3.22 dB. It is found that dipole antennas with the proposed FSS director have a higher gain compared with the conventional dipole antennas without the FSS director at all resonance frequencies. The FSS director in this proposal can transmit the signals covering LTE, Wi-MAX, and WLAN systems moreover, it is clearly seen that the proposed structure has comparable or better results when comparing with other research works in literatures.

V. CONCLUSION

The proposed unit cell is based on the bandpass filter (BPF) structure using aperture interdigital and step-impedance techniques. It can be used for three operating frequency bands, which all bands can be controlled as desired by adjusting the loaded capacitive value at the end of the transmission line. Also, the size of the proposed unit cell is very compact due to the length of the transmission line in the unit cell structure is reduced from λ/2 to λ/8 caused by the slow-wave effect. The proposed unit cells have been used to design the FSS director for the dipole antennas to increase the gains. Also, with the proposed FSS director, the distance between the FSS and the dipole antenna is about λ/8, which is very small compared with the conventional antenna system. The FSS director has the best performance at both E-plane and H-plane in co polarization. The simulation results of dipole antenna with the proposed FSS director at all of frequencies have return loss lesser than −10 dB and the gains in E-plane co-polarization of 4.52 dB at 1.8 GHz, 3.83 dB at 3.7 GHz, and 3.29 dB at 5.2 GHz. In the measured results, the dipole antennas with the proposed FSS director at all resonance frequencies have the return losses lesser than -10 dB and the gains in E-plane co-polarization of 3.67 dB at 1.8 GHz, 3.16 dB at 3.7 GHz, and 3.42 dB at 5.2 GHz, respectively. For H-plane co-polarization, the antenna gains are 3.53 dB at 1.8 GHz, 3.18 dB at 3.7 GHz, and 3.22 dB at 5.2 GHz, respectively. From the design of multiband FSS it can be seen that the simulation results and the measurement results are similar. The proposed FSS director can operate covering LTE, Wi-MAX, and WLAN systems.. However, the proposed FSS director can be also applied for any multi-band wireless communication system such as space technology, especially

it can be used as a part of cover or radome of antenna system for higher gain and compact size.

REFERENCES

[1] S. E. Mendhe and Y. P. Kosta, "Metamaterial properties and applications," *Int. J. Inf. Technol. Knowl. Manag.*, vol. 4, no. 1, pp. 85–89, 2011.

[2] P. Moitra, B. A. Slovick, W. Li, I. I. Kravchencko, D. P. Briggs, S. Krishnamurthy, and J. Valentine, "Large-scale all-dielectric metamaterial perfect reflectors," *ACS Photon.*, vol. 2, no. 6, pp. 692–698, May 2015.

[3] S. Bhattacharyya, D. Chaurasiya, K. V. Srivastava, A. Bhattacharya, and S. Ghosh, "Compact multi-band polarisation-insensitive metamaterial absorber," *IET Microw. Antenna Propag.*, vol. 10, no. 1, pp. 94–101, Jan. 2016.

[4] D. Marathe and K. Kulat, "A compact triple-band negative permittivity metamaterial for C, X-band applications," *Int. J. Antennas Propag.*, vol. 2017, pp. 1–12, Jan. 2017.

[5] W. Kamonsin, P. Krachodnok, P. Chomtong, and P. Akkaraekthalin, "Dual-band metamaterial based on Jerusalem cross structure with interdigital technique for LTE and WLAN systems," *IEEE Access*, vol. 8, pp. 21565–21572, 2020, doi: 10.1109/ACCESS.2020.2968563.

[6] F. Yang and Y. Rahmat-Samii, *Low Profile Wire Antennas on EBG Ground Plane in Electromagnetic Band Gap Structures in Antenna Engineering*. New York, NY, USA: Cambridge Univ. Press, 2009.

[7] A. Kaabal, B. E. Jaafari, S. Ahyoud, and A. Asselman, "Design of EBG antenna with multi-sources excitation for high directivity applications," in *Proc. 11th Int. Conf. Interdisciplinarity Eng., Inter-Eng.*, Tirgu-Mures, Romania, Oct. 2017, pp. 598–604.

[8] P. Jirasakulporn, P. Chomtong, K. Bandudej, and P. Akkaraekthalin, "A compact triple band EBG using interdigital coplanar waveguide structure for antenna gain enhancement," *Int. J. Antennas Propag.*, vol. 2020, pp. 1–18, Dec. 2020, doi: 10.1155/2020/2856807.

[9] A. Chatterjee and S. K. Parui, "Frequency-dependent directive radiation of monopole-dielectric resonator antenna using a conformal frequency selective surface," *IEEE Trans. Antennas Propag.*, vol. 65, no. 5, pp. 2233–2239, May 2017, doi: 10.1109/TAP.2017.2677914.

[10] G. Das, A. Sharma, R. K. Gangwar, and M. S. Sharawi, "Performance improvement of multiband MIMO dielectric resonator antenna system with a partially reflecting surface," *IEEE Antennas Wireless Propag. Lett.*, vol. 18, no. 10, pp. 2105–2109, Oct. 2019, doi: 10.1109/LAWP.2019.2938004.

[11] A. A. Omar and Z. Shen, "Multiband high-order bandstop 3-D frequency-selective structures," *IEEE Trans. Antennas Propag.*, vol. 64, no. 6, pp. 2217–2226, Jun. 2016, doi: 10.1109/TAP.2016.2546967.

[12] R. V. S. R. Krishna and R. Kumar, "Slotted ground microstrip antenna with FSS reflector for high-gain horizontal polarisation," *Electron. Lett.*, vol. 51, no. 8, pp. 599–600, Apr. 2015, doi: 10.1049/el.2015.0339.

[13] B. Doken and M. Kartal, "Easily optimizable dual-band frequency-selective surface design," *IEEE Antennas Wireless Propag. Lett.*, vol. 16, pp. 2979–2982, 2017, doi: 10.1109/LAWP.2017.2756118.

[14] M. J. Huang, M. Y. Lv, J. Huang, and Z. Wu, "A new type of combined element multiband frequency selective surface," *IEEE Trans. Antennas Propag.*, vol. 57, no. 6, pp. 1798–1803, Jun. 2009, doi: 10.1109/TAP.2009.2019910.

[15] A. G. Neto, J. C. E. Silva, J. D. N. Cruz, J. B. D. O. Silva, and N. J. P. D. L. Ramos, "Multiband frequency selective surface with open matryoshka elements," in *Proc. 9th Eur. Conf. Antennas Propag. (EuCAP)*, Apr. 2015, pp. 1–5.

[16] N. Liu, X. Sheng, J. Fan, Y. Wang, and D. Guo, "Reconfigurable frequency selective surface with multiband characteristic," in *Proc. Int. Conf. Electromagn. Adv. Appl. (ICEAA)*, Sep. 2017, pp. 897–899, doi: 10.1109/ICEAA.2017.8065398.

[17] M. Mantash, A. Kesavan, and T. A. Denidni, "Beam-tilting endfire antenna using a single-layer FSS for 5G communication networks," *IEEE Antennas Wireless Propag. Lett.*, vol. 17, no. 1, pp. 29–33, Jan. 2018, doi: 10.1109/LAWP.2017.2772222.

[18] S. Mohamad, R. Cahill, and V. Fusco, "Selective high impedance surface active region loading of Archimedean spiral antenna," *IEEE Antennas Wireless Propag. Lett.*, vol. 13, pp. 810–813, 2014, doi: 10.1109/LAWP.2014.2314860.

[19] A. A. Omar and Z. Shen, "Multi-band second-order bandstop frequency selective structure with controllable band ratios," in *Proc. IEEE Int. Symp. Antennas Propag. USNC/URSI Nat. Radio Sci. Meeting*, Jul. 2015, pp. 1260–1261, doi: 10.1109/APS.2015.7305019.

[20] B. A. Munk, *Frequency-Selective Surface Theory and Design*. New York, NY, USA: Wiley, 2000.

[21] Y. Yuan, K. Zhang, B. Ratni, Q. Song, X. Ding, Q. Wu, S. N. Burokur, and P. Genevet, "Independent phase modulation for quadruplex polarization channels enabled by chirality-assisted geometric-phase metasurfaces," *Nature Commun.*, vol. 11, no. 1, p. 4186, Aug. 2020.

[22] Y. Yuan, K. Zhang, X. Ding, B. Ratni, S. N. Burokur, and Q. Wu, "Complementary transmissive ultra-thin meta-deflectors for broadband polarization-independent refractions in the microwave region," *Photon. Res.*, vol. 7, no. 1, pp. 80–88, 2019, doi: 10.1364/PRJ.7.000080.

[23] K. Zhang, Y. Yuan, X. Ding, H. Li, B. Ratni, Q. Wu, J. Liu, S. N. Burokur, and J. Tan, "Polarization-engineered noninterleaved metasurface for integer and fractional orbital angular momentum multiplexing," *Laser Photon. Rev.*, vol. 15, no. 1, Jan. 2021, Art. no. 2000351, doi: 10.1002/lpor.202000351.

[24] B. Belyaev, A. M. Serzhantov, A. A. Leksikov, Y. F. Bal'va, and A. A. Leksikov, "High-quality compact interdigital microstrip resonator and its application to bandpass filter," *Prog. Electromagn. Res. C*, vol. 72, pp. 91–103, 2017, doi: 10.2528/PIERC16101303.

[25] X. Zhang, Y. Wen, and K. Zhou, "A capacitive loaded quasi-elliptic function microstrip filter on GSM-R band," in *Proc. 3rd IEEE Int. Symp. Microw., Antenna, Propag. EMC Technol. Wireless Commun.*, Oct. 2009, pp. 535–537, doi: 10.1109/MAPE.2009.5355664.

[26] J. Xu, W. Wu, and G. Wei, "Compact multi-band bandpass filters with mixed electric and magnetic coupling using multiple-mode resonator," *IEEE Trans. Microw. Theory Techn.*, vol. 63, no. 12, pp. 3909–3919, Dec. 2015, doi: 10.1109/TMTT.2015.2488643.

[27] H. Jin, K. Wang, J. Guo, S. Ding, and K. Wu, "Slow-wave effect of substrate integrated waveguide patterned with microstrip polyline," *IEEE Trans. Microw. Theory Techn.*, vol. 64, no. 6, pp. 1717–1726, Jun. 2016, doi: 10.1109/TMTT.2016.2559479.

[28] S. Meesomklin, P. Chomtong, and P. Akkaraekthalin, "A compact multiband BPF using step-impedance resonators with interdigital capacitors," *Radioengineering*, vol. 25, no. 2, pp. 258–267, Apr. 2016, doi: 10.13164/re.2016.0258.

[29] P. Chomtong and P. Akkaraekthalin, "A triple-band bandpass filter using Tri-section step-impedance and capacitively loaded step-impedance resonators for GSM, WiMAX, and WLAN systems," *Frequenz*, vol. 68, nos. 5–6, pp. 227–234, 2014, doi: 10.1515/freq-2013-0126.

[30] P. Velez, J. Selga, J. Bonache, and F. Martin, "Slow-wave inductively-loaded electromagnetic bandgap (EBG) coplanar waveguide (CPW) transmission lines and application to compact power dividers," in *Proc. 46th Eur. Microw. Conf. (EuMC)*, Oct. 2016, pp. 104–107, doi: 10.1109/EuMC.2016.7824288.

[31] T. Zhou, Y. Cao, and Z. Cheng, "Compact multiband interdigital-coupled-fed planar antenna with stepped-impedance structures for mobile handsets," *Int. J. Antennas Propag.*, vol. 2017, pp. 1–8, Jan. 2017, doi: 10.1155/2017/7435834.

[32] R. S. Beeresha, A. M. Khan, and R. H. V. Manjunath, "Design and optimization of interdigital capacitor," *Int. J. Res. Eng. Technol.*, vol. 5, no. 33, pp. 73–78, Nov. 2016.

[33] K. Pengthaisong, P. Krachodnok, and R. Wongsan, "Design of a dual-band antenna using a patch and frequency selective surface for WLAN and Wimax," in *Proc. 10th Int. Conf. Electr. Eng./Electron., Comput., Telecommun. Inf. Technol.*, May 2013, pp. 1–4, doi: 10.1109/ECTI-Con.2013.6559631.

P. CHOMTONG (Member, IEEE) received the M.Eng. and Ph.D. degrees in electrical engineering from the King Mongkut's University of Technology North Bangkok (KMUTNB), Thailand, in 2006 and 2011, respectively. In 2012, he joined the Department of Teacher Training in Electrical Engineering, KMUTNB, as an Instructor. His current research interests include passive and active microwave circuits, wideband and multiband antennas, and telecommunication systems.

P. KRACHODNOK (Member, IEEE) received the M.Eng. degree in electrical engineering from Chulalongkorn University (CU), Thailand, in 2001, and the Ph.D. degree in telecommunication engineering from the Suranaree University of Technology (SUT), Thailand, in 2008. Since 2001, she has been joining the School of Telecommunication Engineering, SUT. Her experiences & expert are electromagnetic theory, microwave engineering, and antenna engineering.

K. BANDUDEJ received the B.Eng. and M.Eng. degrees from the Mahanakorn University of Technology (MUT). In 2004, he worked as a R&D RF Engineer at Oxtek, Thailand, focused on board band antenna and microwave air cavity multiplexer design for mobile communication. In 2006, he worked at Endwave Corporation as a Senior RF Engineer, in-charge of various RF/microwave transceiver products from 15GHz to 68GHz. In 2011, he worked with Gigoptix Inc., as a Senior RF Engineer, involved in IC packaging design, MMICs characterization, and high data rate products. In 2013, he joined CAD-IT Consultants (Asia) Pte. Ltd. Since 2018, he has been a Senior RF Design Engineer with the Radio Astronomical Research Institute of Thailand (NARIT), Chiang Mai. His research interest includes application of microwave technology.

P. AKKARAEKTHALIN (Member, IEEE) received the B.Eng. and M.Eng. degrees in electrical engineering from the King Mongkut's University of Technology North Bangkok (KMUTNB), Thailand, in 1986 and 1990, respectively, and the Ph.D. degree from the University of Delaware, Newark, USA, in 1998. From 1986 to 1988, he worked with the Microtek Laboratory, Thailand. In 1988, he joined the Department of Electrical and Computer Engineering, KMUTNB. His current research interests include passive and active microwave circuits, wideband and multiband antennas, and telecommunication systems. He is a member of IEICE Japan and ECTI Thailand. He was the Chairperson for the IEEE MTT/AP/ED Thailand Joint Chapter, during 2007 to 2008, and the President of ECTI Association, from 2014 to 2015. He is currently the Head of the Senior Research Scholar Project of Thailand Research Fund (TRF).

● ● ●